Matrix Infrared Spectra and Density Functional Calculations of Manganese and Rhenium Carbonyl Neutral and Anion Complexes

Lester Andrews,* Mingfei Zhou,† and Xuefeng Wang†

Department of Chemistry, University of Virginia, Charlottesville, Virginia 22904-4319

Charles W. Bauschlicher, Jr.

Mail Stop 230−3, NASA Ames Research Center, Moffett Field, California 94035

Received: May 26, 2000

Laser-ablated Mn and Re atoms and electrons react with CO upon co-condensation in excess argon and neon to produce carbonyl neutrals and anions. These species are identified through isotopic substitution, CCl_4 doping to trap ablated electrons, and density functional theory isotopic frequency calculations. MnCO is identified at 1933.6 cm^{-1} in argon and at 1950.7 cm^{-1} in neon, which are in agreement with the gas phase 1955 ± 15 cm^{-1} photoelectron measurement. $MnCO^-$ is found at 1789.4 cm^{-1} in argon and 1807.5 cm^{-1} in neon. The $Mn(CO)_2$ and $Re(CO)_2$ dicarbonyls are major product absorptions. Annealing to allow further reaction of CO produces higher carbonyls including $Mn_2(CO)_{10}$ and $Re_2(CO)_{10}$ in solid argon. Argon and neon matrix experiments are compared for both metals.

Introduction

Transition-metal carbonyls are significant in organometallic chemistry, and these complexes have been investigated thoroughly.[1] Manganese carbonyls are particularly interesting in that the saturated compound is the binuclear metal−metal bonded species $(OC)_5Mn-Mn(CO)_5$, which can be dissociated into $Mn(CO)_5$ radicals in a number of ways including pyrolysis, photolysis, and chemical reactions.[2−5] In an early matrix isolation investigation of thermal manganese atoms with carbon monoxide, Huber et al.[6] reported an infrared spectrum of $Mn(CO)_5$, which was subsequently shown to be incorrect from photochemical studies of $HMn(CO)_5$ in solid CO and argon.[7,8] Further electron spin resonance investigations of $HMn(CO)_5$ photolysis confirmed the $Mn(CO)_5$ radical product and the C_{4v} structure.[9−11] Matrix photolysis of $Mn_2(CO)_{10}$ showed that in addition to Mn−Mn bond dissociation, carbonyl ligands could be expelled to give $Mn_2(CO)_9$ with a low-frequency band for a bridging carbonyl.[12] Dunkin et al. photolyzed $Mn_2(CO)_{10}$ in solid argon and found $Mn_2(CO)_9$ to be the major product with no $Mn(CO)_5$.[13] Perutz has reviewed the photochemistry of manganese carbonyl precursors.[14]

The tentative identification of $Mn(CO)_x$ ($x = 1-5$) species in the Huber et al. work is therefore subject to question, in particular the important MnCO intermediate. Bach et al. could not produce the band assigned earlier to MnCO and raised the possibility that atomic Mn does not bond to CO.[15] In addition, Huber et al. identified absorptions due to $Mn_2(CO)_{10}$ and smaller dimanganese carbonyls,[6] which clearly shows that the Mn/CO system is complicated.

The $Re(CO)_5$ radical was first detected in the mass spectrum of $Re_2(CO)_{10}$ vapor.[16] The infrared spectroscopic situation with $Re(CO)_5$ and $Re_2(CO)_{10}$ is more straightforward as these two species are resolved in the spectrum of Re atom plus CO reaction products.[17]

Theoretical calculations have described MnCO as being weakly bound and predicted a carbonyl frequency somewhat higher than that suggested by Huber et al.[18−20] A recent photoelectron investigation of $MnCO^-$ produced a 1955 ± 15 cm^{-1} fine structure interval,[21] which is in accord with the predictions of high-level calculations for the MnCO fundamental.[22] Bond dissociation energies for larger $Mn(CO)_x$ anions have been determined by collision-induced dissociation studies.[23]

We have found that laser ablation is an effective means of evaporating transition-metal atoms for reactions to form unsaturated carbonyls during condensation in excess argon and neon, and that the use of relatively low laser energy reduces the metal concentration and allows the stabilization of cation and anion carbonyl products.[24−32] Furthermore, the addition of CCl_4 to trap ablated electrons provides a basis for the identification of carbonyl cation and anion species. In addition, density functional calculations predict frequencies of unsaturated transition-metal carbonyls within 1−2% and support identifications from matrix infrared spectra and isotopic shifts. We report here such a study on manganese and rhenium, which shows a complementary relationship between argon and neon matrix hosts for reactive and charged guest species and the importance of close interaction between experimental and computational chemistry.

Experimental Section

Methods. The experiment for laser ablation and matrix isolation spectroscopy has been described in detail previously.[33,34] Briefly, the Nd/YAG laser fundamental (1064 nm, 10 Hz repetition rate, 10 ns pulse width) was focused on the rotating metal target (Mn, Johnson Matthey; Re, Goodfellow Metals) using low energy (1−5 mJ/pulse). Laser-ablated metal atoms were co-deposited with carbon monoxide (0.1, 0.2, 0.5%) in neon onto a 4K or in argon onto a 7K CsI cryogenic window

* E-mail: lsa@virginia.edu.
† Permanent address: Laser Chemistry Institute, Fudan University, Shanghai, P. R. China.

10.1021/jp001943l CCC: $19.00 © 2000 American Chemical Society
Published on Web 09/13/2000

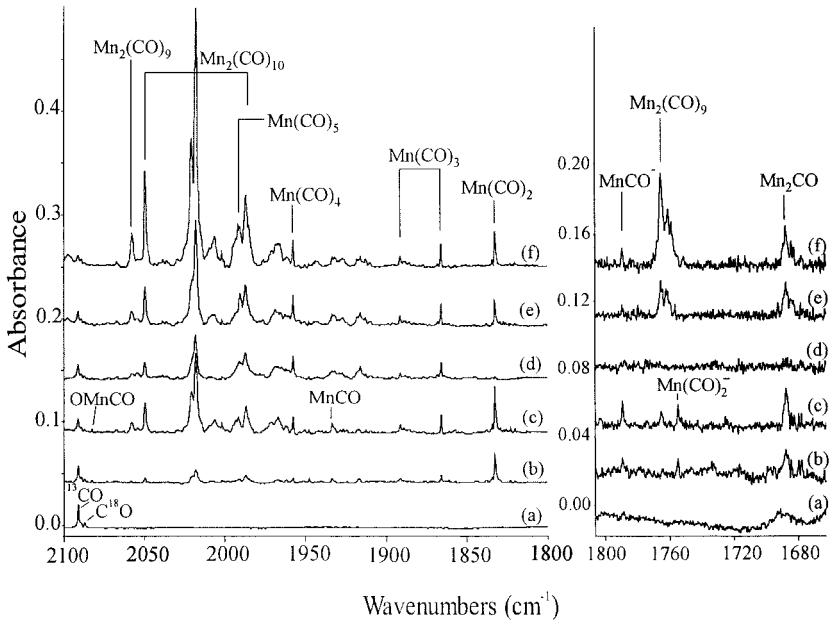

Figure 1. Infrared spectra in the 2100−1800 and 1800−1670 cm^{-1} regions for laser-ablated Mn atoms with 0.2% CO in argon: (a) sample co-deposited for 60 min at 7K, (b) after 30K annealing, (c) after 35K annealing, (d) after $\lambda > 240$ nm photolysis, (e) after 35K annealing, and (f) after 40K annealing.

at 2−4 mmol/hour for 30−60 min. Carbon monoxide (Matheson) and isotopic $^{13}C^{16}O$ and $^{12}C^{18}O$ (Cambridge Isotopic Laboratories) and selected mixtures were used in different experiments. FTIR spectra were recorded at 0.5 cm^{-1} resolution on a Nicolet 750 spectrometer with 0.1 cm^{-1} accuracy using a HgCdTe detector. Matrix samples were annealed stepwise, and selected samples were subjected to photolysis by a medium-pressure mercury arc (Philips, 175 W, globe removed, major lines 240−580 nm but some red light with $\lambda > 630$ nm) using glass filters. Additional experiments were done with CCl_4 added to the sample at 10% of the CO concentration to capture ablated electrons.[26−32]

Results. *Mn + CO in Argon.* Infrared spectra are shown in Figure 1 for the carbonyl region using 0.2% CO in argon, low (~4 mJ/pulse) laser energy, and a 7K substrate: only a very weak absorption was detected at 1832 cm^{-1} after deposition (Figure 1a). Annealing to 20K increased this feature and other very weak bands at 1789.4 and 1754.9 cm^{-1} and produced other absorptions that appear more fully after annealing to 30K (Figure 1(b)). Further annealing to 35K increased the new bands in different proportions; for example, the 1832.5 cm^{-1} band almost doubled, whereas the 2049.7, 2017.8, and 1986.8 cm^{-1} absorptions increased six times (Figure 1c). Photolysis (240−580 nm) affected the bands, which helps in grouping for different product species; for example, the weak 1754.9 and 1789.4 cm^{-1} absorptions disappeared, the 1832.5 cm^{-1} band almost disappeared, the 1891.1 and 1865.7 cm^{-1} bands decreased by 30%, and the 2049.7, 2017.8, and 1986.8 cm^{-1} set decreased by 50% (Figure 1d). Further annealing (Figure 1e,f) recovered most of the band absorbance lost on photolysis, but the last band set more than doubled. Similar experiments were done using approximately 30% higher and lower laser powers. The sharp bands at 1957.6, 1933.6, 1891.1, 1865.7, and 1832.5 cm^{-1} maintained the same relative intensities with the three laser energies; however, the 2049.7, 2017.8, and 1986.8 cm^{-1} set increased relative to the above sharp bands with increasing laser energy. Weak MnO (833.3 cm^{-1})[35] and OMnCO (2082.5 and 869.9 cm^{-1})[36] bands were observed in the spectra.

Similar spectra were obtained with ^{13}CO and $C^{18}O$, and the infrared absorptions are listed in Table 1. Mixed $^{12}CO + {}^{13}CO$ samples gave sharp bands in the 1970−1780 cm^{-1} region, as shown in Figure 2. The 1832.5 cm^{-1} absorption gave a sharp 1/2/1 triplet, the 1865.7 cm^{-1} band produced a quartet, the 1933.6 cm^{-1} band showed a doublet, and the 1957.6 cm^{-1} absorption yielded only pure isotopic bands.

TABLE 1: Infrared Absorptions (cm^{-1}) Observed from Co-Deposition of Laser-Ablated Mn Atoms, Cations, and Electrons with CO in Excess Argon at 10K

^{12}CO	^{13}CO	$C^{18}O$	$^{12}CO/^{13}CO$	$^{16}CO/C^{18}O$	assign
2082.5	2036.5[a]	2033.3	1.022 58	1.024 20	OMnCO
2057.9	2014.9	2007.5	1.02134	1.025 11	$Mn_2(CO)_9$
2049.7	2002.4	2004.6	1.023 62	1.022 50	$Mn_2(CO)_{10}$
2017.8	1972.5	1971.3	1.022 97	1.023 59	$Mn_2(CO)_{10}$
2006.4	1961.4	1960.2	1.022 94	1.023 57	$Mn_x(CO)_y$
1991.8	1948.9	1946.1	1.022 01	1.023 48	$Mn(CO)_5$
1986.8	1943.0	1941.3	1.022 54	1.023 44	$Mn_2(CO)_{10}$
1967	1923	1922	1.022 9	1.023 2	Mn_xCO
1957.6	1890.6[a]	1912.6	1.022 99	1.023 53	$Mn(CO)_4$
1933.6	1913.6[a]	1886.8	1.022 74	1.024 80	MnCO
1915.9	1873.2	1868.4	1.022 80	1.025 42	$Mn_x(CO)_y$
1891.1	1847.8[b]	1849.0	1.023 43	1.022 76	$Mn(CO)_3$
1865.7	1824.3[c]	1822.3	1.022 69	1.023 82	$Mn(CO)_3$
1832.5	1792.5[d]	1788.8	1.022 32	1.024 43	$Mn(CO)_2$
1789.4	1748.0	1747.2	1.023 68	1.024 27	$MnCO^-$
1765.4	1723.8	1728.2	1.024 13	1.021 52	$Mn_2(CO)_9$
1754.9	1714.7		1.023 33		$Mn(CO)_2^-$
1687.5		1645.0		1.02 583	$(Mn_2)CO$
1678.0		1635.8		1.025 80	$(Mn_2)CO$
1515.5	1482.2	1479.5	1.022 47	1.024 33	$(CO)_2^-$
869.9	870.0				OCMnO
833.3	833.3	796.8		1.045 81	MnO
655.3	641.2	652.2	1.021 99	1.004 75	$Mn_2(CO)_{10}$
648.5	635.0	645.1	1.021 26	1.005 27	$Mn_2(CO)_{10}$

[a] Mixed $^{12}CO + {}^{13}CO$ spectrum gave a doublet with no observable intermediate components. [b] Mixed $^{12}CO + {}^{13}CO$ spectrum gave new components at 1988.9, 1986.9, 1863.8, 1861.8 and 1860.3 cm^{-1}. [c] Mixed $^{12}CO + {}^{13}CO$ spectrum gave a quartet with new 1837.7 and 1835.7 cm^{-1} components. [d] Mixed $^{12}CO + {}^{13}CO$ spectrum gave a triplet with new 1809.0 cm^{-1} component.

Mn + CO in Neon. Infrared spectra for the 2100−1840 and 1840−1650 cm^{-1} regions are illustrated in Figure 3 using 0.1% CO in neon at 4K. This figure also shows the effect of CCl_4 additive in the sample for the bottom two traces (a and b) as

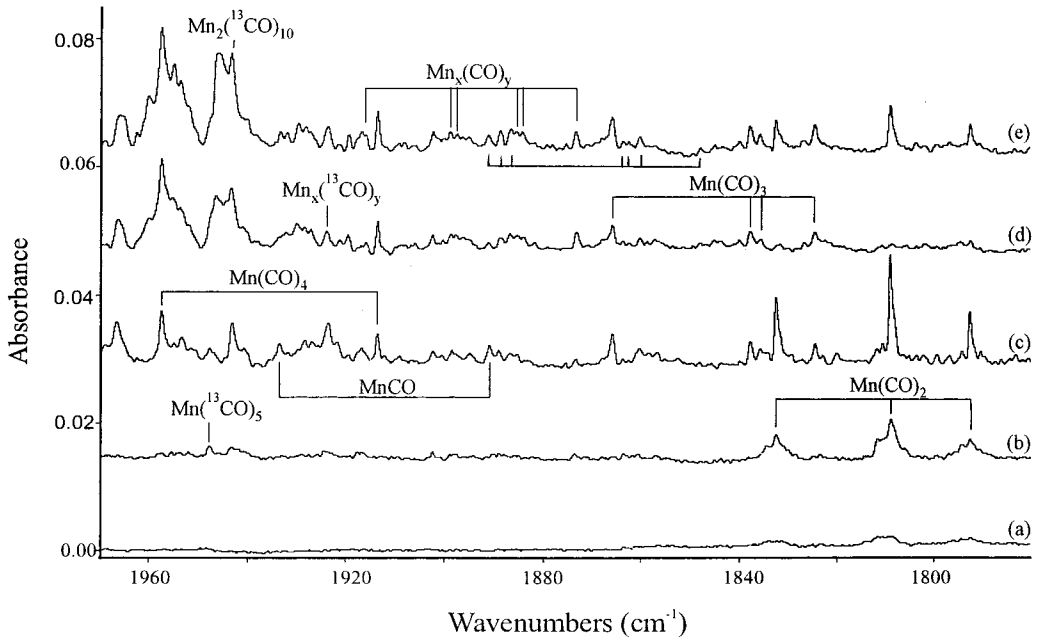

Figure 2. Infrared spectra in the 1970−1780 cm^{-1} region for laser-ablated Mn atoms with 0.1% ^{12}CO + 0.1% ^{13}CO in argon: (a) sample co-deposited for 60 min at 7K, (b) after annealing to 30K, (c) after annealing to 35K, (d) after λ > 240 nm photolysis, and (e) after annealing to 35K.

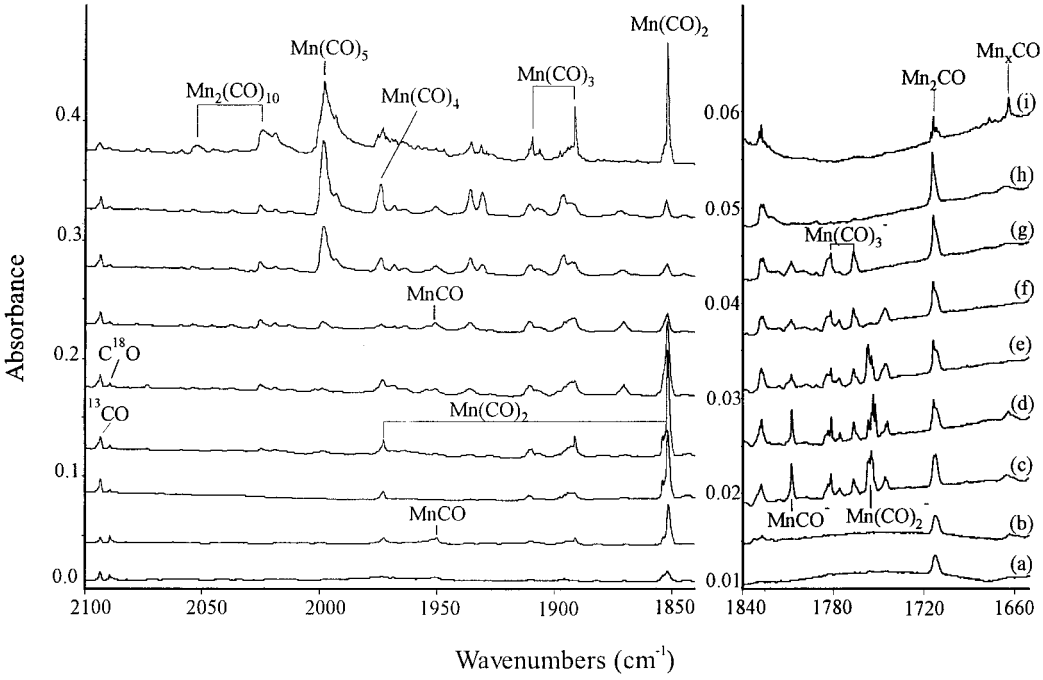

Figure 3. Infrared spectra in the 2100−1840 and 1840−1650 cm^{-1} regions for laser-ablated Mn atoms with 0.1% CO in neon: (a) 0.1% CO with 0.02% CCl_4 co-deposited for 30 min at 4K, (b) after annealing to 8K, (c) 0.1% CO co-deposited for 30 min at 4K, (d) after annealing to 8K, (e) after λ > 630 nm photolysis, (f) after λ > 470 nm photolysis, (g) after λ > 380 nm photolysis, (h) after λ > 290 nm photolysis, and (i) after annealing to 11K.

compared to the second two spectra (c and d): the major product at 1851.5 cm^{-1} is observed on deposition and increases markedly on 8K annealing with an associated 1973.2 cm^{-1} band. However, new bands in the 1840−1740 cm^{-1} region are eliminated with CCl_4 added, and absorptions at 2089.5 and 1950.7 cm^{-1} are increased substantially. Photolysis with a series of long-wavelength pass filters ultimately destroys bands in the 1840−1740 cm^{-1} region and decreases and increases others in the 2100−1840 cm^{-1} region, spectra e−h. Finally, annealing to 11K restored the sharp bands at 1909.5, 1891.1, 1851.5, and 1827.5 cm^{-1}.

Experiments were done with ^{13}CO and $C^{18}O$, and the absorptions are listed in Table 2. Mixed isotopic multiplets in an experiment with ^{12}CO + ^{13}CO sample will be considered with assignments for these absorptions.

Re + CO in Argon. Infrared spectra in the 2110−1690 cm^{-1} region for laser-ablated Re and 0.2% CO in argon co-deposited at 7K are shown in Figure 4. Weak bands in the initial spectrum appear at 1884.0, 1858.5, 1713.7, and 1704.2 cm^{-1}; annealing first to 20K and then to 30K increases these bands and produces new ones at 1958.6 and 1895.9 cm^{-1}. Photolysis destroys the 1713.7−1704.2 cm^{-1} set and the weak 1985.9 cm^{-1} band, and

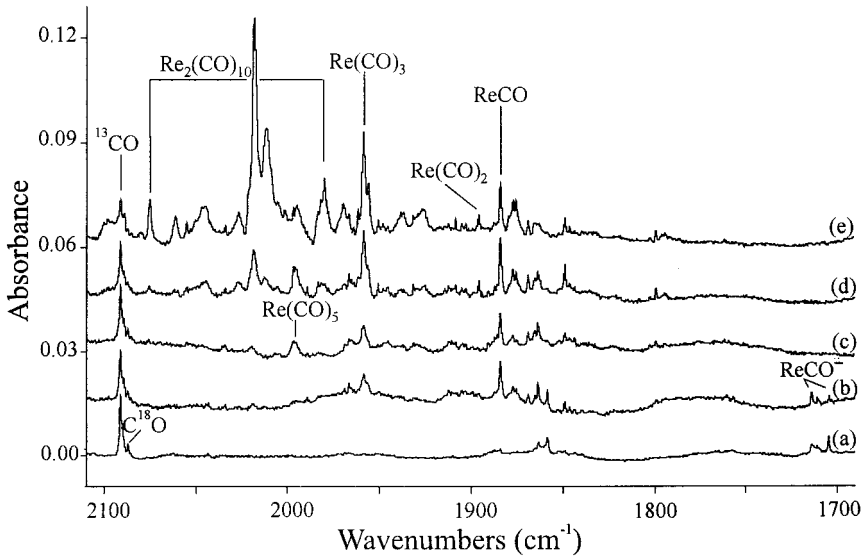

Figure 4. Infrared spectra in the 2110−1690 cm^{-1} region for laser-ablated Re atoms with 0.2% CO in argon: (a) sample co-deposited for 60 min at 7K, (b) after 30K annealing, (c) after $\lambda > 240$ nm photolysis, (d) after 35K annealing, and (e) after 40K annealing.

TABLE 2: Infrared Absorptions (cm^{-1}) Observed from Co-Deposition of Laser-Ablated Mn Atoms, Cations, and Electrons with CO in Excess Neon at 4K

^{12}CO	^{13}CO	$C^{18}O$	$^{12}CO/^{13}CO$	$C^{16}O/C^{18}O$	assign.
2085.9	2039.8	2036.7	1.022 60	1.024 16	OMnCO
2052.6					$Mn_2(CO)_{10}$
2024.4	1979.1	1977.9	1.022 89	1.023 51	$Mn_2(CO)_{10}$
1998.5	1954.1	1951.8	1.022 72	1.023 93	$Mn(CO)_5$
1973.9	1930.7	1927.1	1.022 12	1.024 03	$Mn(CO)_4$
1972.8	1927.0[a]	1929.9	1.023 77	1.022 23	$Mn(CO)_2$, sym
1950.7	1907.0	1906.2	1.022 91	1.023 34	MnCO
1935.6	1892.5	1891.3	1.022 77	1.023 42	$Mn_x(CO)_y$
1930.9	1889.0	1884.1	1.022 18	1.024 84	$Mn_x(CO)_y$
1909.5	1865.8	1866.8	1.023 42	1.022 87	$Mn(CO)_3$, sym
1891.1	1849.2	1846.9	1.022 66	1.023 93	$Mn(CO)_3$, asym
1851.5	1811.3[a]	1807.3	1.022 19	1.024 46	$Mn(CO)_2$, asym
1827.5	1788.7	1782.6	1.021 69	1.025 18	$(Mn(CO)_4^-)$
1807.5	1766.7	1766.4	1.023 09	1.023 27	$MnCO^-$
1783.3	1742.3	1741.7	1.023 59	1.023 88	$Mn(CO)_3^-$ site
1781.8	1741.9	1740.8	1.022 91	1.023 55	$Mn(CO)_3^-$
1766.8	1726.1	1727.9	1.023 58	1.022 51	$Mn(CO)_3^-$ site
1756.2	1716.5	1716.8	1.023 13	1.022 95	$Mn(CO)_2^-$
1753.7	1714.0	1714.3	1.023 16	1.022 98	$Mn(CO)_2^-$ site
1745.7	1706.7	1705.6	1.022 85	1.023 51	$Mn(CO)_2^-$ site
1713.4	1677.5	1670.3	1.021 40	1.025 74	$(Mn_2)CO$
1712.8	1676.3	1669.9	1.021 77	1.025 69	$(Mn_2)CO$ site
1663.7	1628.6	1622.1	1.021 55	1.025 65	$(Mn_x)CO$
1517.4	1482.2	1481.1	1.023 75	1.024 51	$(CO)_2^-$

[a] Mixed isotopic bands at 1953.7 and 1827.6 cm^{-1} in $^{12}CO + ^{13}CO$ experiments.

decreases the 1884.0 cm^{-1} absorption. Subsequent annealing increases and then decreases the 1884.0 cm^{-1} feature while increasing the 1895.9 and 1958.6 cm^{-1} bands. The spectrum after 40K annealing is dominated by the 2018.5 cm^{-1} band and associated absorptions at 2075.2 and 1979.8 cm^{-1} due to $Re_2(CO)_{10}$.[37]

Isotopic precursor experiments were performed, and the observed absorptions are listed in Table 3. Three mixed $^{12}CO+^{13}CO$ investigations were done, and two bands gave triplet systems, namely 1895.9, 1868.7, 1855.0 cm^{-1} and 1958.6, 1938.3, 1914.1 cm^{-1}.

Re + CO in Neon. The carbonyl region for similar rhenium experiments in neon is illustrated in Figure 5. As for manganese, we show 0.1% CO in neon first with 0.01% CCl_4 additive and then without; the 1882.0 cm^{-1} band due to ClCO in neon has

TABLE 3: Infrared Absorptions (cm^{-1}) Observed from Co-Deposition of Laser-Ablated Re Atoms, Cations, and Electrons with CO in Excess Argon at 10K

^{12}CO	^{13}CO	$C^{18}O$	$^{12}CO/^{13}CO$	$C^{16}O/C^{18}O$	assign.
2075.2		2031.1		1.021 71	$Re_2(CO)_{10}$
2018.5		1971.6		1.023 79	$Re_2(CO)_{10}$
1994.8		1948.6		1.023 71	$Re(CO)_5$
1979.8		1935.5		1.022 89	$Re_2(CO)_{10}$
1958.6	1914.1[a]	1914.4	1.023 25	1.023 09	$Re(CO)_3$
1950.7	1906.0	1905.6	1.023 45	1.023 67	$Re(CO)_3$ site
1895.9	1855.0[b]	1853.9	1.022 05	1.022 65	$Re(CO)_2$
1884.0	1839.5	1843.9	1.024 19	1.021 75	ReCO
1868.7	1823.2	1831.7	1.02496	1.020 20	ReCO site
1858.4	1812.7	1821.6	1.025 16	1.020 20	ReCO site
1848.8	1807.9	1808.5	1.022 69	1.022 28	?
1799.1	1756.2	1761.7	1.024 42	1.021 23	?
1713.7	1670.3	1682.4	1.026 04	1.018 60	$ReCO^-$
1710.4	1667.1	1678.8	1.025 97	1.018 82	$ReCO^-$ site
1704.2	1661.0	1672.5	1.026 01	1.018 95	$ReCO^-$

[a] Mixed isotopic band at 1938.3 cm^{-1} in $^{12}CO + ^{13}CO$ experiments. [b] Mixed isotopic band at 1868.7 cm^{-1} in $^{12}CO + ^{13}CO$ experiments.

been observed with other metals.[27] The strongest product absorption at 1905.4 cm^{-1} on deposition is unaffected by CCl_4, but the sharp 2102.1 cm^{-1} band is increased four times and the 1788−1728 cm^{-1} bands are eliminated. The latter bands are destroyed by full-arc photolysis, which produces a strong 2004.0 cm^{-1} absorption and bands in between. Absorptions observed for isotopic precursors are given in Table 4.

Computational Section

Methods. The geometries for anticipated product molecules were optimized, and the harmonic frequencies were computed using the BP86 functional.[38,39] In some cases the hybrid[40] B3LYP[41] functional was employed. For Mn, C, and O, the 6-31+G* basis sets[42−45] and, for Re, the LANL2DZ effective core potential and associated valence basis set[46] were used. The default "extrafine" grid was used in all production calculations. The "ultrafine" grid was employed to confirm that some small distortions from higher symmetry were real and not due to numerical noise. All calculations were performed using Gaussian98.[47]

The computed frequencies are not sufficiently accurate to unambiguously identify the experimental bands. However, we

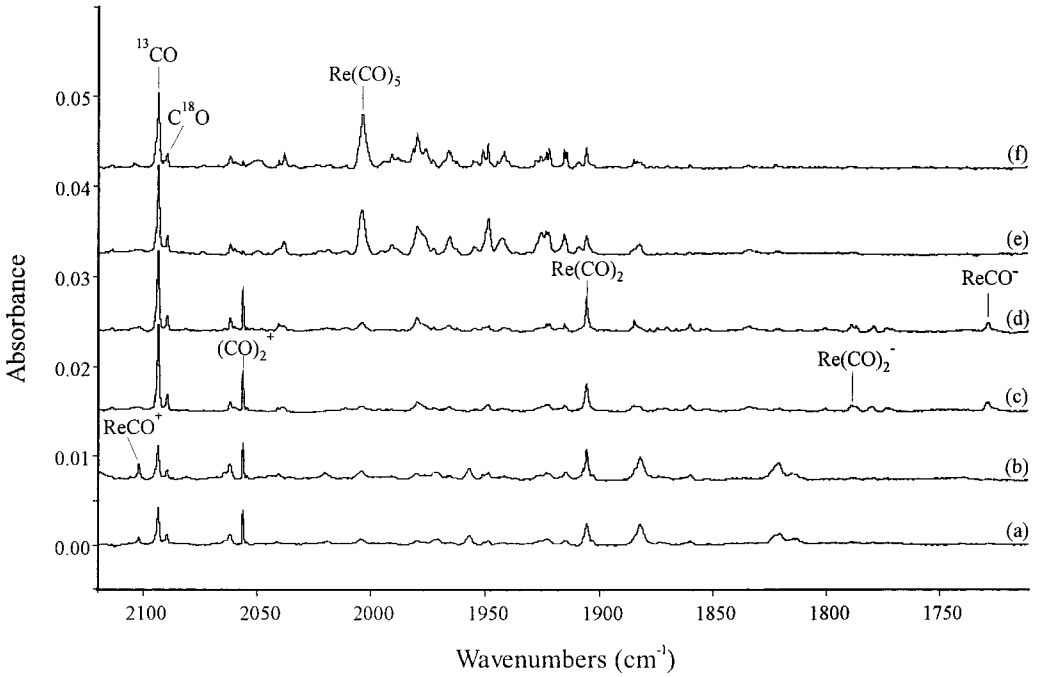

Figure 5. Infrared spectra in the 2200−1700 cm^{-1} regions for laser-ablated Re atoms with 0.1% CO in neon: (a) 0.1% CO with 0.02% CCl_4 co-deposited for 30 min at 4K, (b) after annealing to 8K, (c) 0.1% CO co-deposited for 30 min at 4K, (d) after annealing to 8K, (e) after $\lambda > 240$ nm photolysis, (f) after annealing to 10K.

TABLE 4: Infrared Absorptions (cm^{-1}) Observed from Co-Deposition of Laser-Ablated Re Atoms, Cations, and Electrons with CO in Excess Neon at 4K

^{12}CO	^{13}CO	$C^{18}O$	$^{12}CO/^{13}CO$	$C^{16}O/C^{18}O$	assign.
2102.1	2056.5	2051.4	1.022 17	1.024 71	$ReCO^+$
2056.3	2010.9	2007.4	1.022 58	1.024 36	$(CO)_2^+$
2023	1978	1977	1.022 8	1.023 3	$Re_2(CO)_{10}$
2004.0	1959.3	1957.2	1.023 02	1.023 92	$Re(CO)_5$
1979.8	1935.4	1933.3	1.022 94	1.024 05	$Re_x(CO)_y$
1948.7	1906.0	1902.0	1.022 40	1.024 55	$Re_x(CO)_y$
1923.3	1878.4	1880.6	1.023 90	1.022 70	$Re_x(CO)_y$
1915.3	1871.3	1872.8	1.023 51	1.022 69	$Re_x(CO)_y$
1905.4	1863.8	1859.9	1.022 32	1.024 46	$Re(CO)_2$
1884.5	1843.4	1839.3	1.022 30	1.024 57	? (Re)(CO)
1860.1	1818.8	1818.0	1.022 70	1.023 16	? (Re)(CO)
1788.7	1747.1	1750.0	1.023 81	1.022 11	$Re(CO)_2^-$
1778.8	1738.9	1738.2	1.022 95	1.023 36	$Re(CO)_x^-$
1728.0	1684.0	1693.9	1.026 12	1.020 13	$ReCO^-$

have found that the ratios of the isotopic frequencies characterize normal modes and help to identify new molecular species. Therefore, we computed the isotopic frequencies for ^{13}CO and $C^{18}O$ and the $^{12}CO/^{13}CO$ and $C^{16}O/C^{18}O$ frequency ratios, and use these ratios in conjunction with the computed frequencies to aid in the identification of the experimental bands.

Our experience has been that the BP86 functional is biased in favor of states with higher d occupations and lower spin. Thus, the lowest state found in the BP86 approach many not be the true ground state. For this reason, the geometries were optimized for several states, and the computed frequencies for the lowest state of each spin were compared with experiment to determine ground state. Because of the BP86 bias toward low-spin states, if a state with a multiplicity of M is higher in energy than a state with multiplicity of M + 2, states with lower multiplicities are not considered.

In addition to the bias with multiplicity, the BP86 approach is biased toward states with higher d populations. As more CO molecules are added, the number of low-lying states decreases and their d populations become more similar; therefore the BP86 approach is expected to become more reliable with increasing number of CO molecules. Despite these limitations, previously, we have found the BP86 functional to give the best results for systems containing transition metals, i.e., calculated harmonic frequencies in close agreement with the experimental fundamentals.[26−32] However, as we discuss below, for the MnCO system, we were unable to interpret experiments using the BP86 results, and we were forced to consider the B3LYP approach as well.

We should also note that caution must be used in finding the ground state, and we commonly switched occupied and virtual orbitals to confirm that the state under consideration was in fact the ground state. We commonly computed in no symmetry, and only performed the final calculation with symmetry.

Results. The ground state of Mn is ^6S ($3d^54s^2$). The interaction with CO is expected to be weak because of the repulsion between the CO 5σ and the Mn 4s orbitals. Bending of the MnCO angle can reduce the repulsion, but this reduces the overlap of the Mn 3dπ and CO 2π* orbitals. Promotion of the 4s electrons to the 3d orbital can reduce the σ repulsion and increase the number of 3dπ electrons for back-donation; however, the cost of this electron promotion can be high. As more CO molecules are added to share the cost of this promotion, it becomes increasingly favorable. Thus we expect a decrease in the spin with increasing number of CO molecules.

For MnCO at the BP86 level of theory, we find the ground state to be $^4\Sigma^-$. We are unable to obtain a solution for the $^4\Pi$ state, and the $^6\Pi$ state has an imaginary frequency. Thus, the BP86 results appear to be inconsistent with the previous high-level treatment,[22] and the computed frequencies and isotopic shifts do not agree with experiment, thus suggesting that the BP86 approach is biased against the ground state of MnCO. Therefore, we also apply the B3LYP approach to this molecule. At this level, we find the lowest state to be $^6\Pi$, with the $^4\Pi$ state about 5 kcal/mol higher in energy. We are also able to obtain a solution for the $^4\Sigma^-$ state, and it is above the $^4\Pi$ state. Thus, the order of the states at the B3LYP level of theory is more consistent with the higher level of theory. Unfortunately, the B3LYP approach places MnCO above the Mn + CO

TABLE 5: Frequencies (cm^{-1}) and Intensities (km/mol) Calculated for MnCO Species at the BP86/6-311G* Level

molecule		frequencies (intensities)				isotope[a]
CO	$^1\Sigma^+$	2111 (72)				12
MnCO	$^6A'$	1955.5 (441)	363.9 (12)	79.1 (24)		12
		1910.6	359.5	76.9		13
		1910.2	355.8	78.1		18
$^4\Sigma^-$[b]	1865.3 (603)	585.7 (0.4)	356.3 (17 × 2)	12		
1826.9	570.5	352.3	18			
1819.6	580.3	345.5	13			
$Mn(CO)_2$	$^4A_2$	1974.2 (141)	1861.2 (2585)	498.5 (3)		12−12
		1955.1	1836.2	493.3		12−13
		1927.5	1819.7	487.9		13−13
		1930.7	1816.5	492.5		18−18
	$^6B_1$[c]	1956 (212)	1855 (1996)	438 (4)		12−12
$Mn(CO)_3$	$^4A''$	2033.0 (91)	1964.6 (746)	1922.8 (2163)		12−(12)−12
		2024.8	1958.2	1892.2		12−(12)−13
		2015.6	1936.8	1922.4		12−(13)−12
		2025.1	1954.6	1895.4		13−(12)−12
		2002.3	1936.2	1891.1		12−(13)−13
		2017.4	1933.1	1879.4		13−(12)−13
		2002.0	1932.5	1895.0		13−(13)−12
		1985.6	1919.3	1879.3		13−(13)−13
		1987.2	1919.6	1877.4		18−(18)−18
	$^2A''$[d]	2027.5 (15)	1927.1 (2100)	1919.4 (633)		12−(12)−12
		1979.0	1883.6	1873.5		13−(13)−13
		1983.6	1881.5	1877.8		18−(18)−18
$Mn(CO)_4$	$^2B_2$	2047.0 (9)	1961.6 (448)	1957.1 (1737)	1938.0 (1262)	12
	$^4A_2$[e]	2034.1 (0)	1955.1 (1280 × 3)			12
		1986.9,	1910.8			13
		1989.7,	1909.1			18
$Mn(CO)_5$	$^2A_1$	2077 (0, a_1)	1997 (0, b_2)	1982 (3164, e)	1981 (801, a_1)	12
$MnCO^-$	$^5A'$	1813.2 (838)	376.6 (3)	153.3 (28)		12
		1771.4	372.1	148.9		13
		1771.5	368.3	151.2		18
	$^5\Sigma$[f]	1711 (642)	497 (83)	280 (14)	269 (8)	12
$Mn(CO)_2^-$	$^3B_1$	1861.5 (200)	1770.8 (2920)	529.6 (96)		12
		1815.7	1729.9	525.4		13
		1822.9	1730.4	520.0		18
	$^3B_2$	1777 (728)	1709 (1890)	573 (1)		12
	$^5B_1$[g]	1826 (1099)	1780 (1777)	460 (273)		12
$Mn(CO)_3^-$	$^3A_2$	1864.3 (378)	1774.3 (167 × 2)			12
		1819.5	1732.2			13
		1824.4	1735.5			18
$Mn(CO)_4^-$	$^3B_1$	1928 (72)	1843 (915)	1834 (1295)		12
	$^1A_1$[h]	1924 (96)	1821 (1871)	1818 (1676)	1818 (1295)	12
$Mn(CO)_5^-$	$^1A_1$	1987 (0)	1893 (1907)	1888 (0)	1867 (1610 × 2)	12
$MnCO^+$	$^7\Sigma^+$	2196.6 (14)	146.5 (34)	93.2 (4 × 2)		12
		2147.2	144.9	90.6		13
		2144.3	143.2	91.8		18
	$^5\Sigma^-$[i]	2182 (187)	324 (3)	263 (0.1 × 2)		12
$MnCO^+$	$^7\Sigma$	2235 (20)	136 (35)	134 (4 × 2)		12
B3LYP						
MnCO	$^6\Pi$	2019.0 (644)	350.9 (16)	139.1 (13)	110.0 (25)	12
		1972.7	347.1	135.1	106.8	13
		1972.3	342.7	137.1	108.6	18
	$^4\Sigma^-$	1921 (944)	565 (4)	345 (17 × 2)		12
	$^4\Pi$[j]	2020 (1124)	399 (5)	228 (6 × 2)		12
$MnCO^-$	$^5\Pi$	1875 (807)	288 (15)	115 (7)	112 (62)	12

[a] Isotope: 12 = ^{12}CO, 13 = ^{13}CO, 18 = $C^{18}O$. [b] $^4\Sigma^-$ state is 6.3 kcal/mol lower than $^6A'$ state at BP86 level. [c] $^6B_1$ state is 25.9 kcal/mol higher than $^4A_2$ state. [d] $^2A''$ state is 0.5 kcal/mol lower than $^4A''$, but BP86 is biased in favor of the doublet state. [e] $^4A_2$ state is 9.5 kcal/mol above $^2B_2$ state, but experimental spectra favor the $^4A_2$ state with one strong infrared absorption. [f] $^5\Sigma$ state is 6.8 kcal/mol lower than $^5A'$ state at BP86 level. [g] $^3B_2$ state is 8.8 kcal/mol and $^5B_1$ state is 34.9 kcal/mol above $^3B_1$ state. [h] $^1A_1$ state is 5.0 kcal/mol above $^3B_1$ state. [i] $^5\Sigma$ is 3.9 kcal/mol above $^7\Sigma$ state. [j] $^4\Sigma^-$ state is +6.4 kcal/mol and $^4\Pi$ state is +5.0 kcal/mol above the $^6\Pi$ state at the at B3LYP level.

asymptote. A comparison of the results with experiment supports the assignment of the ground state as $^6\Pi$; thus, this appears to be one of those cases where the B3LYP functional works better for a transition-metal system than the BP86 approach, although the slightly bent (170.2°) $^6A'$ state computed by BP86 has a 1955.5 cm^{-1} fundamental and isotopic ratios in very close agreement with the 1950.7 cm^{-1} neon matrix value. The calculated harmonic frequencies and intensities are summarized in Table 5. Figure 6 illustrates the computed structures.

For $Mn(CO)_2$, we find the lowest state to be $^4A_2$, which is 25.9 kcal/mol below the $^6B_1$ state despite any bias in the BP86 approach; this energy difference is sufficiently large that we can be confident that the ground state is $^4A_2$. The computed results are consistent with experiment so we did not consider the B3LYP approach.

For $Mn(CO)_3$, we find the $^4A''$ state to be the lowest, which is only 0.5 kcal/mol below the lowest doublet state. Since the BP86 tends to favor the low-spin state, we conclude that $^4A''$

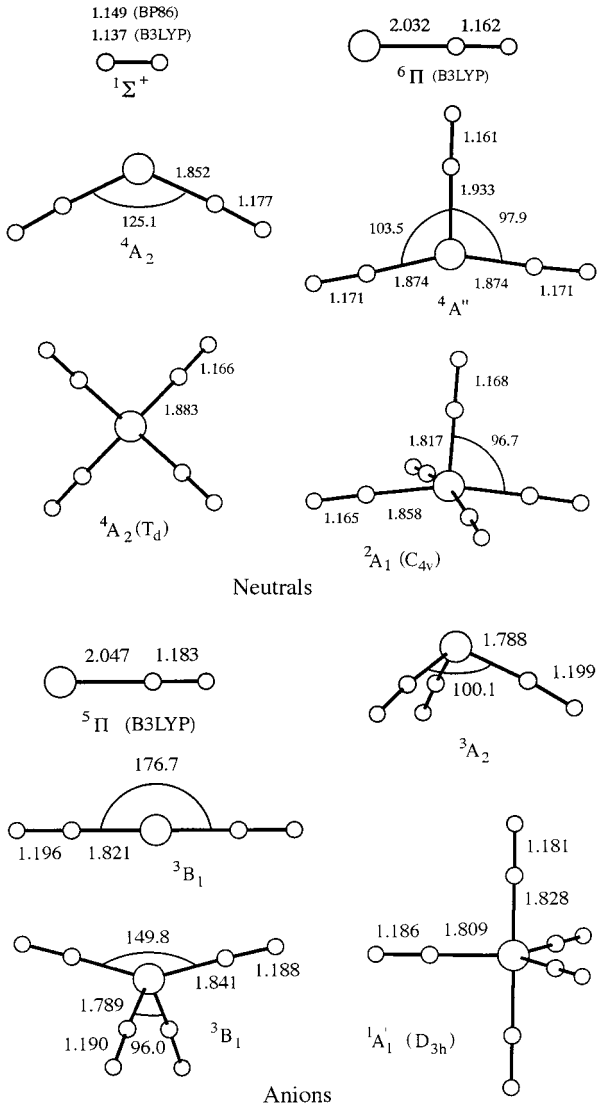

Figure 6. Structural diagrams for manganese carbonyl neutrals and anions computed by DFT (BP86 except where noted B3LYP).

is the ground state, which is consistent with experiment. The $^4A''$ state is T-shaped and only very slightly distorted from C_{2v} symmetry. The energy lowering (0.01 kcal/mol) by reducing the symmetry from C_{2v} to C_s is so small that we reran the C_{2v} geometry using improved grids, but in all cases, the C_{2v} structure had an imaginary frequency. Consistent with the very small energy change, the two structures have very similar frequencies, excluding the lowest frequency, which changes from imaginary to real as the symmetry is lowered. Thus, while we cannot exclude the possibility that the system really has C_{2v} symmetry, we are still safely able to compare the computed frequencies with experiment.

For $Mn(CO)_4$, we find two low-lying states, a $^4A_2$ state with a tetrahedral structure which is 9.5 kcal/mol above a $^2B_2$ state with C_{2v} symmetry. This doublet state is best viewed as arising from a square−planar structure and bending two opposing CO out of the plane and two below the plane. The experimental spectrum is more compatible with the $^4A_2$ state, even though it is higher in energy. $Mn(CO)_5$ is a square pyramid with a $^2A_1$ ground state.

For $MnCO^-$, the BP86 functional yields a $^5\Sigma^-$ ground state; the $^5\Pi$ state is higher in energy and has an imaginary frequency. The B3LYP approach yields a $^5\Pi$ ground state, and the computed frequencies are in agreement with those from the experiment. Thus, the BP86 approach suffers from the same problems as those found for MnCO. The $^7\Pi$ state is slightly higher in energy.[22]

For $Mn(CO)_2^-$, the ground state is computed to be $^3B_1$, which is only slightly bent. Like $Mn(CO)_3$, we find the higher symmetry structure, in this case the $^3\Sigma_g^-$ state, to be only slightly higher in energy, and we suspect the true ground state is $^3\Sigma_g^-$ with an occupation of $3d\delta^2$.

For $Mn(CO)_3^-$, the calculations predict the ground $^3A_2$ state to have C_{3v} symmetry, which is 12.3 kcal/mol below the lowest quintet state. Experiment confirms this assignment. For $Mn(CO)_4^-$, we find two low-lying states, $^3B_1$ and $^1A_1'$, both have C_{2v} symmetry and are derived from distorting the square. We find the $^3B_1$ state to be 5 kcal/mol below $^1A_1$, and since BP86 favors low-spin states, we conclude that the ground state is $^3B_1$. Finally, $Mn(CO)_5^-$ is a trigonal bipyramid with an $^1A_1'$ ground state.

Similar calculations were done for ReCO and $Re(CO)_2$ species, and the results are reported in Table 6. In contrast to MnCO, ReCO has the $^4\Sigma^-$ ground state.

Discussion

The new product absorptions will be assigned on the basis of argon and neon matrix spectra, isotopic shifts and multiplet splittings, and the density functional theory calculated isotopic frequencies.

$Mn(CO)_x$, $x = 1-5$. The argon matrix spectra are dominated after annealing by strong bands at 2049.7, 2017.8, and 1986.8 cm^{-1} that are due to $Mn_2(CO)_{10}$, based on the spectrum of an authentic sample,[6] and bands at 1687.5 and 1678.0 cm^{-1} that agree with Huber et al. for $(Mn_2)CO$. The sharp intermediate bands at 1957.6, 1933.6, 1891.1, 1865.7, and 1832.5 cm^{-1} maintain constant relative intensities with themselves and the 1991.8 cm^{-1} $Mn(CO)_5$ radical band[8] on increasing laser energy (and Mn atom concentration), which favors the former dimanganese species. The above new sharp bands are therefore due to monomanganese carbonyls, which will be identified from the mixed $^{12}CO + {}^{13}CO$ spectra.

The 1933.6 cm^{-1} band and its 1950.7 cm^{-1} neon matrix counterpart are in very good agreement with the 1955 ± 15 cm^{-1} MnCO fundamental from the photoelectron spectrum.[21] The 1955.5 cm^{-1} frequency for the $^6A'$ ground-state MnCO complex by BP86 and $^6\Pi$ ground state 2019.0 cm^{-1} prediction by B3LYP are compatible with this assignment based on the scale factors 0.998 and 0.966, which are typical for BP86 and B3LYP, respectively.[27-31] Our BP86 and B3LYP calculations also predict 364 and 351 cm^{-1}, respectively, for the ground-state Mn−CO fundamental deduced at 370 ± 20 cm^{-1} from the photoelectron spectrum.[21] The ground state is probably $^6\Pi$ as predicted by earlier CASSCF/ICACPF calculations.[22] The 1933.6 cm^{-1} band forms a 1:1 doublet with mixed $^{12}CO + {}^{13}CO$ (Figure 2) for the vibration of a single carbonyl. It is interesting to note that the MnCO band was enhanced with CCl_4 additive in solid neon; this is due to the prevention of MnCO loss through electron capture. A similar effect has been found for ScCO.[24] The 2089.5 cm^{-1} band, also enhanced with CCl_4, might be due to a cation, but there is insufficient evidence for an assignment.

The 1832.5 cm^{-1} argon and 1851.5 cm^{-1} neon matrix bands dominate sample deposition and the early stages of annealing in both matrices (Figures 1 and 3). Note that more diffusion and reaction takes place on co-deposition in neon at 4K than in argon at 7K. The 1851.5 cm^{-1} band is sufficiently strong on 8K annealing to track with a weaker 1972.8 cm^{-1} band. The

TABLE 6: Frequencies (cm^{-1}) and Intensities (km/mol) Calculated for ReCO Species

molecule		frequencies (intensities)				isotope[a]
ReCO[b]	$^4\Sigma^-$	1880.6 (676)	602.0 (2)	422.1 (5)	420.6 (5)	12
(BP86)		1832.9	594.8	409.2	407.8	13
		1844.1	581.5	417.1	415.7	18
	^{6}A″	1880.2 (670)	413.4 (17)	136.8 (77)		12
		1837.3	405.5	133.4		13
		1836.4	403.3	134.1		18
ReCO[b]	$^4\Sigma^-$	1941.7 (922)	594.4 (6)	434.6 (5)	425.4 (5)	12
(B3LYP)		1893.7 (872)	586.9	421.2	412.5	12
		1902.2	574.7	429.5	420.3	18
	^{6}A″	1979 (832)	391 (12)	120 (76)		12
Re(CO)$_2$[c]	$^4\Sigma_g^-$	2013.5 (0)	1907.0 (2355)	600.3 (5)		12
(BP86)		1964.4 (0)	1864.0 (2220)	580.2 (4)		13
		1971.4 (0)	1861.9 (2288)	596.6 (4)		18
	^{4}A$_2$	1944.4 (263)	1854.4 (2037)	526.7 (0.2)		12
		1897.4 (250)	1812.4 (1912)	512.5 (0.01)		13
		1903.1 (254)	1810.8 (1991)	521.5 (0.5)		18
ReCO$^-$[d]	$^5\Sigma^-$	1742.1 (805)	547.9 (47)	308.5 (100)	306.3 (94)	12
(BP86)		1697.7	541.3	299.1	296.9	13
		1708.5	529.1	305.0	302.6	18
	$^5\Pi$	1765.8 (890)	529.6 (15)	491.6 (189)	400.2 (0.5)	12
ReCO$^-$[d]	$^5\Sigma^-$	1796.1 (1015)	546.3 (41)	326.7 (85)	325.8 (82)	12
(B3LYP)		1751.1	539.5	316.7	315.8	12
		1760.3	527.9	322.8	322.0	18
	$^5\Pi$	1824	545	516	408	12
Re(CO)$_2^-$	$^3\Sigma^-$	1906.1 (0)	1783.3 (2965)	530.8 (13 × 2)		12
(BP86)		1858.4	1742.2	513.5		13
		1869.0	1742.3	526.6		18
Re(CO)$_2^-$	$^3\Sigma^-$	1980.9 (0)	1843.6 (3748)	553.6 (12 × 2)		12
(B3LYP)		1932.0	1801.8	535.5		13
		1940.4	1800.2	549.4		18
ReCO$^+$	$^5\Pi$	2023.6 (267)	504.3 (7)	391.4 (2)	352.0 (0)	12
(BP86)		1976.0	497.3	397.6	341.4	13
		1978.8	488.4	386.5	347.5	18

[a] Isotope: 12 = ^{12}CO, 13 = ^{13}CO, 18 = C^{18}O. [b] ^{6}A″ is 35.6 and 31.5 kcal/mol higher than $^4\Sigma^-$ at BP86 and B3LYP levels, respectively. [c] ^{4}A$_2$ is 13.8 kcal/mol higher than $^4\Sigma^-$ at BP86 level. [d] $^5\Pi$ is 26.9 and 28.8 kcal/mol higher than $^5\Sigma^-$ at BP86 and B3LYP levels, respectively.

strong bands form 1:2:1 triplets in both ^{12}CO + ^{13}CO experiments so two equivalent carbonyls are involved; the 1972.8, 1953.7, 1927.0 cm^{-1} and 1851.5, 1827.6, 1811.3 cm^{-1} triplets in solid neon are asymmetric in that the central components are displaced blue and red, respectively, by the same 3.8 cm^{-1} due to interaction between the symmetric and antisymmetric stretching modes for Mn(^{12}CO)(^{13}CO). The DFT calculations predict 1974.2 cm^{-1} a_1 and 1861.2 cm^{-1} b_2 vibrations of 141/2585 relative intensity for ^{4}A$_2$ ground-state Mn(CO)$_2$, which are in excellent agreement with the neon matrix frequencies and the acceptable agreement with the relative intensity. The ^{12}CO/^{13}CO and C^{16}O/C^{18}O frequency ratios are slightly different for these symmetric and antisymmetric modes (Table 2), and the DFT frequency (Table 5) ratios model this characteristic difference in carbon and oxygen participation for each mode.

The sharp 1891.1/1865.7 cm^{-1} argon matrix and 1909.5/1891.1 cm^{-1} neon matrix band pairs track together on annealing and photolysis, which favor the higher carbonyls. The 1891.1/1865.7 cm^{-1} pair appears next on annealing after Mn(CO)$_2$ but before the sharp 1957.6 cm^{-1} absorption. DFT calculations predict two strong C−O stretching modes for ^{4}A″ planar, almost T-shaped Mn(CO)$_3$ at 1964.6 and 1922.8 cm^{-1} with 746/2163 relative intensity, which are in very good agreement with the matrix observations including the observed 1/2.7 relative intensity. The ^{12}CO + ^{13}CO experiment (Figure 2) shows a complicated mixed isotopic pattern that nicely matches the calculated mixed isotopic frequencies. For the stronger 1865.7 cm^{-1} band, a quartet with two central components separated by 2.0 cm^{-1} is observed; the eight calculated frequencies form four bands within the line width and central components separated by 3.5 cm^{-1}, in good agreement with the observed quartet. For the weaker 1891.1 cm^{-1} band, a higher multiplet is observed; the eight calculated frequencies have only one coincidence and seven bands are observed in surprising agreement with the calculations. This excellent agreement for two fundamentals confirms the identification of Mn(CO)$_3$.

Our DFT calculations find a ^{2}A″ Mn(CO)$_3$ state almost degenerate with the above ^{4}A″ state. However, the symmetric and stronger antisymmetric C−O modes are reversed in position such that these calculated frequencies and isotopic ratios do not match the observed bands and isotopic frequency ratios.

The sharp 1957.6 cm^{-1} argon and 1973.9 cm^{-1} neon matrix bands come next and have no related bands. In solid neon, the 1973.9 and 1998.5 cm^{-1} bands were markedly increased on photolysis at the expense of Mn(CO)$_{2,3}$. Further annealing produced more Mn(CO)$_{2,3}$ and decreased the 1973.9 cm^{-1} band in favor of a broader 1998.5 cm^{-1} band. The 1957.6 cm^{-1} argon and 1973.9 cm^{-1} neon matrix bands are assigned to Mn(CO)$_4$. Our BP86 calculations find two states for Mn(CO)$_4$, and the ^{4}A$_2$ state degenerate frequency calculated at 1955.1 cm^{-1} matches the one-band spectrum better than the ^{2}B$_2$ state with two observable infrared absorptions.

The 1991.8 cm^{-1} argon and 1998.5 cm^{-1} neon matrix bands appear on annealing. The former is in agreement with the argon matrix band produced by HMn(CO)$_5$ photolysis, and the latter is near the 2000 cm^{-1} gas-phase Mn(CO)$_5$ measurement.[48] The mixed isotopic neon experiment gave a strong doublet, which is appropriate for the degenerate mode of a high-symmetry

species.[49] Our DFT calculation predicted a doublet-state square−planar molecule, in agreement with previous investigations,[7,9−11] and a strong (e) mode at 1981.4 and (a_1) mode at 1980.8 cm^{-1}. In neon, we see only one band at 1998.5 cm^{-1} for $Mn(CO)_5$, and $Mn_2(CO)_{10}$ gives only a weak band at 2025.3 cm^{-1} so there is no complication with the 1998.5 cm^{-1} band as found for the argon matrix counterpart. In the CO matrix[7] the e and a_1 modes were assigned as 1987.6 and 1978.4 cm^{-1}. The a_1 mode may be a shoulder at 1988 cm^{-1}, but we cannot be certain.

$Mn_2(CO)_x$ Species. The 2049.7, 2017.8, 1986.8 cm^{-1} bands[6] of $Mn_2(CO)_{10}$ dominate the argon matrix spectrum after 35K annealing. In addition, bands that appear on late annealing at 2057.9 and 1765.4 cm^{-1} agree with 2058 and 1764 cm^{-1} absorptions reported by Dunkin et al. for $Mn_2(CO)_9$ with a semibridging carbonyl group formed by 296 ± 5 nm photolysis of $Mn_2(CO)_{10}$ in solid argon.[13] In our mixed $^{12}CO + {}^{13}CO$ experiment, the 1765.4 cm^{-1} band became a 1:1 doublet at 1764.9, 1723.8 cm^{-1}, indicating the vibration of one CO subunit (the semibridged CO) coupled very slightly to other carbonyls. Further broadband photolysis gave a new 2068 cm^{-1} band from the photoejection of at least one more CO[13]; this band is observed here on late annealing at 2067.0 cm^{-1}. Finally, we also observe bands at 1687.5, 1678.0 cm^{-1} on early annealing, essentially the same as that assigned by Huber et al. to bridged $(Mn_2)CO$.[6] The 1713.4 cm^{-1} neon matrix counterpart was sharp; the $^{12}CO + {}^{13}CO$ spectrum gave the same (±0.1 cm^{-1}) bands in a 1:1 doublet. A similar band appeared at 1663.7 cm^{-1} on annealing in neon and gave a sharp, mixed isotopic doublet for a monocarbonyl species in presumably a larger metal cluster.

Manganese Carbonyl Anions. Photosensitive bands in the 1740−1840 cm^{-1} region in solid neon were eliminated on doping with CCl_4 to serve as an electron trap, whereas the $(Mn_2)CO$ 1713.4 cm^{-1} band remained with CCl_4 and increased on photolysis. The former bands behave as carbonyl anions did in similar Fe, Co, Ni, and Cu experiments.[24−32] Absorptions due to $(CO)_2^-$ and $(CO)_2^+$ were also observed in these experiments.[24−32,50]

The 1807.5 cm^{-1} band exhibits only ^{12}CO and ^{13}CO counterparts in $^{12}CO + {}^{13}CO$ experiments, whereas the 1756.2 cm^{-1} band forms a 1:2:1 triplet with 1731.8 cm^{-1} intermediate component. Our BP86 calculations predict $^5A'$ $MnCO^-$ at 1831.2 cm^{-1} and 25.0 kcal/mol below $^6A'$ MnCO, and the B3LYP functional finds the $^5\Pi$ state anion at 1874.7 cm^{-1} and 24.0 kcal/mol below $^6\Pi$ MnCO, which are in excellent agreement with the 1807.5 cm^{-1} neon matrix band and the 25.7 kcal/mol gas-phase electron affinity (EA).[21,22] The 1807.5 cm^{-1} neon and 1789.4 cm^{-1} argon matrix bands are assigned to $MnCO^-$.

The 1756.2 cm^{-1} band is in good agreement with the DFT prediction of a very strong 1770.8 cm^{-1} band for $^3B_1$ $Mn(CO)_2^-$, and the band is assigned accordingly. We cannot, however, locate the a_1 mode predicted about 90 cm^{-1} higher with 7% of the 1756.2 cm^{-1} band intensity.

Photolysis with $\lambda > 630$ nm radiation first decreases $MnCO^-$ with little effect on $Mn(CO)_2^-$, and then $\lambda > 470$ nm irradiation destroyed $Mn(CO)_2^-$ without an increase in the 1766.8 cm^{-1} absorptions in this region. The DFT energy differences for $Mn(CO)_2$ and $Mn(CO)_2^-$ predict a slightly higher EA for the dicarbonyl (38.2 kcal/mol) consistent with requiring shorter wavelength radiation for photodetachment. Then, $\lambda > 380$ nm photolysis destroyed the 1745.9 cm^{-1} band and increased slightly the remaining 1781.9 and 1766.8 cm^{-1} bands, and finally, the latter bands were destroyed by $\lambda > 290$ nm radiation, which increased the 1712.8 cm^{-1} $(Mn_2)CO$ cluster absorption. Subsequent $\lambda > 240$ nm photolysis destroyed the 1827.5 cm^{-1} band. The latter bands are probably due to $Mn(CO)_x^-$ anions, but x is difficult to determine. The 1745.7 cm^{-1} band is likely a matrix site of $Mn(CO)_2^-$.

Recall that the stable $Mn(CO)_5^-$ anion absorbs at 1898 and 1863 cm^{-1} in THF solution,[51] which is in excellent agreement with our calculated bands at 1893 and 1867 cm^{-1}. Furthermore, the calculated energy differences predict a high 70.8 kcal/mol EA for $Mn(CO)_5$. We find no photosensitive bands in the 1850−1950 cm^{-1} region for $Mn(CO)_5^-$; apparently annealing to reach penta coordination allows charge recombination−neutralization. Our DFT calculation predicts $Mn(CO)_3^-$ to be a $^3A_2$ C_{3v} species, 12.9 kcal/mol below the quintet state and 51.3 kcal/mol below $Mn(CO)_3$, and to have a very strong e mode at 1774 cm^{-1}. On the other hand, DFT finds $Mn(CO)_4^-$ to be a $^3B_1$ structure, that is 61.9 kcal/mol below the $Mn(CO)_4$ $^2B_2$ state, and with strong 1832, 1834, and 1842 cm^{-1} infrared absorptions. The latter calculated bands are probably too high for the observed 1781.9 and 1766.8 cm^{-1} absorptions, but the 1774 cm^{-1} prediction for $Mn(CO)_3^-$ is in very good agreement with the observed bands, so the latter bands are assigned accordingly. The separation could be due to matrix sites or to splitting of the degenerate mode by symmetry lowering. The 1827.5 cm^{-1} band, however, is in the region expected for $Mn(CO)_4^-$. The band is destroyed by $\lambda > 240$ nm photolysis but restored on 11K annealing. The 12/13 and 16/18 ratios indicate a C−O mode strongly coupled to metal, but isotopic dilution prevents the observation of a mixed isotopic multiplet. The 1827.5 cm^{-1} band is tentatively assigned to $Mn(CO)_4^-$.

$Re(CO)_x$, $x = 1-5$. The neon matrix spectra are dominated by a sharp 1905.1 cm^{-1} band, which increases on annealing and gives way on photolysis to other bands including the strongest new feature at 2004.0 cm^{-1}. The 2004.0 cm^{-1} band is appropriate for the neon matrix counterpart of the 1995 cm^{-1} argon matrix band for $Re(CO)_5$.[17] A very weak 2023 cm^{-1} feature that appears on annealing with $Re(CO)_5$ is probably due to $Re_2(CO)_{10}$ as the strongest argon matrix absorption is at 2019.7 cm^{-1}.[37]

The 1905.1 cm^{-1} band becomes a 1905.1, 1880.6, 1863.8 cm^{-1} 1:2:1 triplet with mixed $^{12}CO + {}^{13}CO$, which indicates a dicarbonyl vibration. Our DFT calculation predicts the strong σ_u fundamental for $Re(CO)_2$ at 1907.0 cm^{-1}, which supports assignment of the 1905.1 cm^{-1} band to $Re(CO)_2$. The remaining bands that increase on photolysis are probably due to intermediate $Re(CO)_y$ and $Re_2(CO)_y$ species that cannot be identified here owing to lack of resolution of the mixed $^{12}CO + {}^{13}CO$ components.

The initial argon matrix spectra are dominated by sharp 1884.0 and 1858.5 cm^{-1} bands. These features shift to 1839.5 and 1812.7 cm^{-1} with ^{13}CO and show no intermediate components with $^{12}CO + {}^{13}CO$. The $^{12}CO/{}^{13}CO$ ratios 1.02419 and 1.02516 are near the values of the ratio (1.02602) computed for the 1880.6 cm^{-1} fundamental of $^4\Sigma^-$ ReCO, and these bands are best assigned to ReCO in different argon matrix sites. High-level calculations have predicted a $^4\Sigma^-$ ground state for ReCO.[52] Annealing produces a sharp 1895.9 cm^{-1} band, which appears to be the argon matrix counterpart of the 1905.4 cm^{-1} neon matrix $Re(CO)_2$ band; the calculated and observed isotopic frequency ratios are more like CO values. The 1958.6 cm^{-1} band shows an intermediate component with $^{12}CO + {}^{13}CO$ and is appropriate for a possible T-shaped $Re(CO)_3$ molecule. The 1994.8 cm^{-1} band is in agreement with a previous assignment to $Re(CO)_5$ in solid CO.[17] On final 40K annealing, the strong 2018.5 cm^{-1} band and related 2075.2, 1979.8 cm^{-1} bands are

in ±1 cm^{-1} agreement with the argon matrix spectrum of an authentic $Re_2(CO)_{10}$ sample.[37]

Where then, is the neon matrix absorption for ReCO, which is expected as a precursor for $Re(CO)_2$ and $Re(CO)_5$? This question cannot be answered definitively. Weak bands at 1884.5 and 1860.1 cm^{-1} sharpen on annealing, and the former broadens on photolysis while the latter decreases. Both of these bands exhibit isotopic ratios near more conventional CO values, as DFT calculations predict for $^6A''$ ReCO, which is not the ground state. In any case, when two CO molecules become available to Re in solid neon, $Re(CO)_2$ is formed.

Rhenium Carbonyl Anions and Cation. Three photosensitive bands in the 1700 cm^{-1} region in solid neon were not produced with CCl_4 additive; these bands therefore must be considered for anions. The 1728.0 cm^{-1} band forms a 1:1 doublet with $^{12}CO + {}^{13}CO$, so a monocarbonyl is indicated, whereas 1:2:1 triplets appear at 1788.7, 1757.5, 1747.1 cm^{-1} and at 1778.6, 1755.5, 1738.2 cm^{-1} for dicarbonyl species. These bands are assigned to $ReCO^-$ and $Re(CO)_2^-$, respectively. The 1713.7−1704.2 cm^{-1} argon matrix band is also due to $ReCO^-$.

Our DFT calculations predict a $^5\Sigma^-$ ground state for $ReCO^-$ with 1742.1 cm^{-1} (BP86) and 1796.1 cm^{-1} (B3LYP) fundamentals. These frequency calculations support assignment of the 1728.0 cm^{-1} band to $ReCO^-$ (scale factors 0.992, BP86; 0.962, B3LYP). The observed isotopic $^{12}CO/^{13}CO$, $C^{16}O/C^{18}O$ frequency ratios (1.02612, 1.02013) match the calculated ratios (BP86 - 1.02615, 1.01967; B3LYP - 1.02570, 1.02034) and indicate substantial metal−carbon coupling and a strong Re−C bond. On the other hand, the calculations predict a $^3\Sigma^-$ state for $Re(CO)_2^-$ with more conventional isotopic frequency ratios that are in good agreement with the observed (Tables 3 and 4) values.

The sharp 2102.1 cm^{-1} band increased 4-fold with CCl_4 additive; the band increased on early annealing and decreased on photolysis as does other MCO^+ cation absorptions. The ^{13}CO and $C^{18}O$ frequencies and isotopic frequency ratios are appropriate for a relatively uncoupled C−O vibration as observed for OsCO at 2106.0 cm^{-1} and for $IrCO^+$ at 2156.5 cm^{-1}.[27,29] This band increases on 8K annealing and then decreased on photolysis, the same behavior found for other MCO^+ species in similar experiments.[24−32] Accordingly, the 2102.1 cm^{-1} band is assigned to $ReCO^+$ in solid neon.

The assignment is supported by BP86 calculations, which predict a $^5\Pi$ ground state for $ReCO^+$ with a 2023.6 cm^{-1} fundamental. At first, this calculation falling low is surprising, but similar calculations for $OsCO^+$ and $IrCO^+$ are low by 11.8 and 28.3 cm^{-1}. The DFT calculations for these three third-row metal carbonyl cations all predict more M−C coupling (as suggested by higher 12/13 and lower 16/18 ratios) than is observed.[27,29]

Reactions in Neon and Argon Matrixes. Reagent cocondensation in neon at 4K and in argon at 7K allows for considerably different amounts of initial reagent reaction, as a comparison of Figures 1 and 3 indicates. Under these conditions, argon freezes more rapidly and traps the reagents, which can diffuse and react on annealing the matrix, but neon solidifies less rapidly and allows more reagent diffusion and reaction during condensation. Thus, the initial product yield is higher in neon matrix experiments. However, annealing in neon cannot progress beyond about 11K, and the yield of $Mn_2(CO)_{10}$ is much smaller than that of $Mn(CO)_5$ on the basis of the product bands. However, in argon, annealing to 40K gives much stronger $Mn_2(CO)_{10}$ absorptions. The CCl_4 additive prevents the reactions of eqs 2 and 3 by the preferential trapping of ablated electrons. The more controlled annealing in solid argon allows the tricarbonyl and tetracarbonyl products to be identified. Likewise, the anion adds more coordinating carbonyls in exothermic reactions[23] on annealing. The following reactions occur for Mn in both matrices; analogous reactions probably occur for Re but not all of the products have been identified.

$$Mn(^6S) + CO(^1\Sigma) \rightarrow MnCO(^6A') \quad \Delta E = -10.4 \text{ kcal/mol (BP86)} \quad (1)$$

$$MnCO(^6A') + e^- \rightarrow MnCO^-(^5A') \quad \Delta E = -25.0 \text{ kcal/mol (BP86)} \quad (2)$$

$$MnCO(^6\Pi) + e^- \rightarrow MnCO^-(^5\Pi) \quad \Delta E = -24.0 \text{ kcal/mol (B3LYP)} \quad (3)$$

$$MnCO(^6A') + CO \rightarrow Mn(CO)_2(^4A_2) \quad \Delta E = -42.8 \text{ kcal/mol (BP86)} \quad (4)$$

$$Mn(CO)_2(^4A_2) + CO \rightarrow Mn(CO)_3(^4A'') \quad \Delta E = -37.8 \text{ kcal/mol (BP86)} \quad (5)$$

$$Mn(CO)_3(^4A'') + CO \rightarrow Mn(CO)_4(^4A_2) \quad \Delta E = -35.0 \text{ kcal/mol (BP86)} \quad (6)$$

$$Mn(CO)_4(^4A_2) + CO \rightarrow Mn(CO)_5(^2A_1) \quad \Delta E = -56.4 \text{ kcal/mol (BP86)} \quad (7)$$

$$Mn(CO)^-(^5\Pi) + 1,2,3CO \rightarrow Mn(CO)_{2,3,4}^- \quad (8)$$

The higher temperatures attained on annealing solid argon allow the diffusion and dimerization of higher manganese carbonyls. The $Mn_2(CO)_{10}$ and $Mn_2(CO)_9$ bands observed here are in agreement with previous reports.[6,13]

$$Mn(CO)_4 + Mn(CO)_5 \rightarrow Mn_2(CO)_9 \quad (9)$$

$$Mn(CO)_5 + Mn(CO)_5 \rightarrow (OC)_5Mn-Mn(CO)_5 \quad (10)$$

Conclusions

Laser-ablated Mn and Re atoms and electrons react with CO upon co-condensation in excess argon and neon to produce the carbonyl neutral and anion complexes. These species are identified through isotopic substitution, CCl_4 doping to trap ablated electrons, and density functional theory isotopic frequency calculations. MnCO is identified at 1933.6 cm^{-1} in argon and at 1950.7 cm^{-1} in neon, which are in agreement with the gas phase 1955 ± 15 cm^{-1} photoelectron measurement.[21,22] $MnCO^-$ is found at 1789.4 cm^{-1} in argon and 1807.5 cm^{-1} in neon. The $Mn(CO)_2$ and $Re(CO)_2$ dicarbonyls are major product absorptions. The use of density functional theory mixed isotopic molecule frequency calculations to match the argon matrix observations of two stretching modes for $Mn(CO)_3$ is noteworthy. A close working relationship between computational and experimental chemistry is necessary to identify most absorptions in these complicated matrix systems.

Acknowledgment. We gratefully acknowledge N.S.F. support for this research under Grant CHE 97-00116.

References and Notes

(1) Cotton, F. A.; Wilkinson, G.; Murillo, C. A.; Bochmann, M. *Advanced Inorganic Chemistry*, 6th ed.; Wiley: New York, 1999.

(2) Bidinosti, D. R.; McIntyre, W. S. *Can. J. Chem.* **1970**, *48*, 593.
(3) Hallock, S. A.; Wojcicki, A. *J. Organomet. Chem.* **1973**, *54*, C27.
(4) Fawcett, J. P.; Poë, A. J.; Twigg, M. V. *J. Organomet. Chem.* **1973**, *51*, C17.
(5) Haines, L. I. B.; Poë, A. J. *Nature (London)* **1967**, *215*, 699; **1968**, *218*, 562.
(6) Huber, H.; Kundig, E. P.; Ozin, G. A.; Poe, A. J. *J. Am. Chem. Soc.* **1975**, *97*, 308 (Mn + CO).
(7) Church, S. P.; Poliakoff, M.; Timney, J. A.; Turner, J. J. *J. Am. Chem. Soc.* **1981**, *103*, 7515.
(8) Church, S. P.; Poliakoff, M.; Timney, J. A.; Turner, J. J. *Inorg. Chem.* **1983**, *22*, 3259; *J. Mol. Struct.* **1982**, *80*, 159.
(9) Howard, J. A.; Morton, J. R.; Preston, K. F. *Chem. Phys. Lett.* **1981**, *83*, 226.
(10) Symons, M. C. R.; Sweany, R. L. *Organomet.* **1982**, *1*, 834.
(11) Fairhurst, S. A.; Morton, J. R.; Perutz, R.; Preston, K. F. *Organomet.* **1984**, *3*, 1389.
(12) Hepp, A. F.; Wrighton, M. S. *J. Am. Chem. Soc.* **1983**, *105*, 5934.
(13) Dunkin, I. R.; Härter, P.; Shields, C. J. *J. Am. Chem. Soc.* **1984**, *106*, 7248.
(14) Perutz, R. N. Inorganic and Organometallic Photochemistry. In *Chemistry and Physics of Matrix Isolated Species*; Andrews, L., Moskovits, M., Eds.; North-Holland, Amsterdam, 1989; Chapter 9.
(15) Bach, S. B. H.; Taylor, C. A.; Van Zee, R. J.; Vala, M. T.; Weltner, W., Jr. *J. Am. Chem. Soc.* **1986**, *108*, 7104.
(16) Junk, G. A.; Svec, H. J.; *J. Chem. Soc. A* **1970**, 2102.
(17) Huber, H.; Kundig, E. P.; Ozin, G. A. *J. Am. Chem. Soc.* **1974**, *96*, 5585 (Re + CO).
(18) Barnes, L. A.; Bauschlicher, C. W., Jr. *J. Chem. Phys.* **1989**, *91*, 314.
(19) Fournier, R. *J. Chem. Phys.* **1993**, *99*, 1801; *98*, 8041.
(20) Adamo, C.; Lelj, F. *J. Chem. Phys.* **1995**, *103*, 10605.
(21) Fenn, P. T.; Leopold, D. G., unpublished data as quoted by Bauschlicher.[22]
(22) Bauschlicher, C. W., Jr. *Chem. Phys. Lett.* **1996**, *249*, 244 (MnCO).
(23) Sunderlin, L. S.; Wang, D.; Squires, R. R. *J. Am. Chem. Soc.* **1993**, *115*, 12060.
(24) Zhou, M. F.; Andrews, L. *J. Phys. Chem. A* **1999**, *103*, 2964 (Sc + CO).
(25) Zhou, M. F.; Andrews, L. *J. Phys. Chem. A*, **1999**, *103*, 5259 (Ti, V + CO).
(26) Zhou, M. F.; Chertihin, G. V.; Andrews, L. *J. Chem. Phys.* **1998**, *109*, 10893; Zhou, M. F.; Andrews, L. *J. Chem. Phys.* **1999**, *110*, 10370 (Fe + CO).
(27) Zhou, M. F.; Andrews, L. *J. Phys. Chem. A* **1999**, *103*, 6956 (Ru, Ir + CO).
(28) Zhou, M. F.; Andrews, L. *J. Phys Chem. A* **1998**, *102*,10250. The $CoCO^-$ state is $^3\Delta$ (Co + CO).
(29) Zhou, M. F.; Andrews, L. *J. Phys. Chem. A* **1999**, *103*, 7773 (Co, Rh, Ir + CO in Ne).
(30) Zhou, M. F.; Andrews, L. *J. Am. Chem. Soc.* **1998**, *120*, 11499 (Ni + CO).
(31) Liang, B. Y.; Zhou, M. F.; Andrews, L. *J. Phys. Chem. A* **2000**, *104*, 3905. (Ni, Pd, Pt + CO in Ne)
(32) Zhou, M. F.; Andrews, L. *J. Chem. Phys.* **1999**, *111*, 4548 (Cu + CO).
(33) Burkholder, T. R.; Andrews, L. *J. Chem. Phys.* **1991**, *95*, 8697.
(34) Hassanzadeh, P.; Andrews, L. *J. Phys. Chem.* **1992**, *96*, 9177.
(35) Chertihin, G. V.; Andrews, L. *J. Phys. Chem. A* **1997**, *101*, 8547 (Mn + O_2).
(36) Zhou, M. F.; Liang, B.; Andrews, L. *J. Phys. Chem. A* **1999**, *103*, 2013.
(37) Klotzbûcher, W. E. *J. Mol. Struct.* **1988**, *174*, 5.
(38) Becke, A. D. *Phys. Rev. A* **1988**, *38*, 3098.
(39) Perdew, J. P. *Phys. Rev. B* **1986**, *33*, 8822; *34*, 7406(E).
(40) Becke, A. D. *J. Chem. Phys.* **1993**, *98*, 5648.
(41) Stephens, P. J.; Devlin, F. J.; Chabalowski, C. F.; Frisch, M. J. *J. Phys. Chem.* **1994**, *98*, 11623.
(42) Frisch, M. J.; Pople, J. A.; Binkley, J. S. *J. Chem. Phys.* **1984**, *80*, 3265 and references therein.
(43) Wachters, A. J. H. *J. Chem. Phys.* **1970**, *52*, 1033.
(44) Hay, P. J. *J. Chem. Phys.* **1977**, *66*, 4377.
(45) Raghavachari, K.; Trucks, G. W.; *J. Chem. Phys.* **1989**, *91*, 1062.
(46) Wadt, W. R.; Hay, P. J. *J. Chem. Phys.* **1985**, *82*, 284; 299.
(47) Frisch, M. J.; Trucks, G. W.; Schlegel, H. B.; Scuseria, G. E.; Robb, M. A.; Cheeseman, J. R.; Zakrzewski, V. G.; Montgomery, J. A., Jr.; Stratmann, R. E.; Burant, J. C.; Dapprich, S.; Millam, J. M.; Daniels, A. D.; Kudin, K. N.; Strain, M. C.; Farkas, O.; Tomasi, J.; Barone, V.; Cossi, M.; Cammi, R.; Mennucci, B.; Pomelli, C.; Adamo, C.; Clifford, S.; Ochterski, J.; Petersson, G. A.; Ayala, P. Y.; Cui, Q.; Morokuma, K.; Malick, D. K.; Rabuck, A. D.; Raghavachari, K.; Foresman, J. B.; Cioslowski, J.; Ortiz, J. V.; Baboul, A. G.; Stefanov, B. B.; Liu, G.; Liashenko, A.; Piskorz, P.; Komaromi, I.; Gomperts, R.; Martin, R. L.; Fox, D. J.; Keith, T.; Al-Laham, M. A.; Peng, C. Y.; Nanayakkara, A.; Gonzalez, C.; Challacombe, M.; Gill, P. M. W.; Johnson, B.; Chen, W.; Wong, M. W.; Andres, J. L.; Gonzalez, C.; Head-Gordon, M.; Replogle, E. S.; Pople, J. A. *Gaussian 98*, rev. A.7; Gaussian, Inc.: Pittsburgh, PA, 1998.
(48) Seder, T. A.; Church, S. P.; Weitz, E. *J. Am. Chem. Soc.* **1986**, *108*, 7518.
(49) Darling, J. H.; Ogden, J. S. *J. Chem. Soc., Dalton Trans.* **1972**, 2496.
(50) Thompson, W. E.; Jacox, M. E. *J. Chem. Phys.* **1991**, *95*, 735.
(51) Breeze, P. A.; Burdett, J. K.; Turner, J. J. *Inorg. Chem.* **1981**, *20*, 3369.
(52) Tan, H.; Liao, M.; Dai, D.; Balasubramanian, K. *J. Phys. Chem. A* **1999**, *103*, 3495 (ReCO).